Silicon based plasmonic coupler

Roney Thomas,* Zoran Ikonic, and R.W. Kelsall

Institute of Microwave and Photonics, School of Electronic and Electrical Engineering, University of Leeds, Leeds LS2 9JT, United Kingdom.

*el07rt@leeds.ac.uk

Abstract: Plasmonics is a field in which the light matter interaction can be controlled at the nanoscale by patterning the material surface to achieve enhanced optical effects. Realisation of micron sized silicon based plasmonic devices will require efficient coupling of light from an optical fibre grating coupler into silicon compatible plasmonic waveguides. In this paper we have investigated a silicon based plasmonic coupler with a very short taper length, which confines and focuses light from a broad input fibre opening into a plasmonic waveguide at the apex of the structure. A simple transfer matrix model was also developed to analyse the transmission performance of the coupler with respect to its key physical parameters. The proposed plasmonic coupler was optimised with respect to its different structural parameters using finite element simulations. A maximum coupling efficiency of 72% for light coupling from a 6.2μm wide input opening into a 20nm slit width was predicted. The simulated result also predicted an insertion loss of $\approx$ 2.0dB for light coupling into a 300nm single mode SOI waveguide from a plasmonic structure with a 10.4μm input opening width and a taper length of only 3.15μm. Furthermore, the application of the optimised plasmonic coupler as a splitter was investigated, in which the structure simultaneously splits and couples light with a predicted coupling efficiency of $\approx$ 37 % (or a total coupling efficiency of 73%) from a 6.22μm input opening into two 50nm wide plasmonic waveguides.

OCIS codes: (250.5403) Plasmonics; (240.6680) Surface plasmons; (230.0250) Optoelectroncis.

References and links

1. E. Ozbay, "Plasmonics: merging photonics and electronics at nanoscale dimensions," Science **311**, 189–193 (2006).
2. T. Ebssen and C. Genet, "Light in tiny holes," Nature **445**, 39–46 (2007).
3. J. Dionne, L. Sweatlock, M. Sheldon, A. Alivisatos, and H. Atwater, "Silicon based plasmonics for on-chip photonics," IEEE J. of Sel. Top. in Quantum Electron. **16**, 295–306 (2010).
4. O. Janssen, H. Urbach, and G. Hooft, "On the phase of plasmons excited by slits in a metal film," Opt. Express **14**, 11823–11832 (2006).
5. L. H. Thio T, T. Ebbesen, K. Pellerin, G. Lewen, A. Nahata, and R. Limke, "Giant optical transmission of subwavelength apertures: physics and applications," Nanotech. **13**, 429–432 (2002).
6. F. Vidal, H. Lezec, T. Ebbesen, and L. Moreno, "Multiple paths to enhance optical transmission through a single subwavelength slit," Phys. Rev. Lett. **90**, 213901 (2003).
7. T. Thio, K. Pellerin, and R. Linke, "Enhanced ligh transmission through single subwavelength aperture," Opt. Lett. **26**, 1972–1974 (2001).
8. S. Palacios, O. Mahboub, G. Vidal, L. Moreno, S. Rodrigi, C. Genet, and T. Ebbesen, "Mechanisms for extraordinary transmission through bull's eye structures," Opt. Express **19**, 10429–10442 (2011).

#170627 - $15.00 USD Received 18 Jun 2012; revised 17 Aug 2012; accepted 26 Aug 2012; published 5 Sep 2012

9. H. Lezec, A. Degiron, R. Linke, M. Moreno, F. Vidal, and T. Ebbesen, "Beaming light from a subwavelength aperture," Science **297**, 820–822 (2002).
10. H. Ghaemi, T. Thio, G. D.E, T. Ebbesen, and H. Lezec, "Surface plasmons enhanced optical transmission through subwavelength holes," Phys. Rev. B **58**, 6779–6782 (1998).
11. F. Vidal, H. Lezec, T. Ebbesen, and M. Moreno, "Light passing through subwavelength apertures," Rev. Mod. Phys. **82**, 729–787 (2010).
12. T. Sondergaard, S. Bozhevolnyi, S. Novikov, J. Beermann, E. Devaux, and Ebbesen, "Extraordinary optical transmission enhanced by nanofocusing," Nano Lett. **10**, 3123–3128 (2010).
13. O. T. A. Janssen, H. P. Urbach, and G. W. Hooft, "Giant optical transmission of a subwavelength slit optimised using the magnetic field phase," Phys. Rev. Lett. **99**, 043902 (2007).
14. L. Yin, V.-V. V.K, J. Pearson, J. Hiller, J. Hua, U. Welp, D. Brown, and C. Kimball, "Subwavelength focusing and guiding of surface plasmons," Nano Lett. **5**, 1399–1402 (2005).
15. H. Lezec and T. Thio, "Diffracted evanescent model for enhanced and suppressed optical transmission through subwavelength hole arrays," Opt. Express **12**, 3629–3651 (2004).
16. G. Li and A. Xu, "Phase shifts of plasmons excited by slits in a metal film illuminated by oblique incident TM plane wave," Proc. SPIE **7135**, 71350T–9 (2008).
17. L. G. Yuan, C. Lin, X. Feng, and X. An-Shi, "Plasmonic corrugated horn structure for optical transmission enhancement," Chin. Phys. Lett. **26**, 124205 (2009).
18. C. Mentzer, and L. Peters, "Pattern analysis of corrugated horn antennas," IEEE Tran. on Ant. and Prop. **24**, 304–309 (1976).
19. S. Sederberg, V. Van, and A. Ellezabi, "Monolithic integration of plasmonic waveguides into complimentary metal-oxide-semiconductor and photonic compatible platform," Appl. Phys. Lett. **96**, 121101 (2010).
20. Comsol Multiphysics, *www.comsol.com*, 3^{rd} edition.
21. P. Johnson and R. Christy, "Optical constants of noble metals," Phys. Rev. B **6**, 4370–4379 (1972).
22. X. Huang and M. Brongersma, "Rapid computation of light scattering from aperiodic plasmonic structures," Phys. Rev. B **84**, 245120 (2011).
23. M. Kuttge, F. Garcia, and A. Polamn, "How grooves reflect and confine surface plasmon polaritons," Opt. Express **17**, 10385–10392 (2009).
24. J. Galan, P. Sanchis, B. Sanchez, and J. Marti, "Polarisation insensitive fibre to SOI waveguide experimental coupling technique integrated with a v-groove structure," Group IV Photonics, 4th IEEE International Conference, 1–3 (2007).
25. H. Sun, A. Chen, A. Szep, and L. R. Dalton, "Efficient fibre coupler for vertical silicon slot waveguides," Opt. Express **17**, 22571–22577 (2009).
26. K. Shiraishi, M. Kagaya, K. Muro, H. Yoda, Y. Kogami, and C. Tsai, "Single mode fibre with a plano-convex silicon microlens for integrated butt-coupling scheme," Opt. Express **47**, 6345–6349 (2008).
27. S. Zhu, G. Q. Lo, and D. L. Kwong, "Theoretical investigation of silicon MOS-type plasmonic slot waveguide based MZI modulators," Opt. Express **18**, 27802–27819 (2010).
28. R. Thomas, Z. Ikonic, and R. Kelsall, "Electro-optic metal-insulator-semiconductor-insulator-metal Mach-Zehnder plasmonic modulator," Phot. and Nanostructres **10**, 183–189 (2011).

1. Introduction

With the current trend in photonic devices moving towards sub-wavelength dimensions, the field of plasmonics plays an important role in overcoming the diffraction limit with its ability to confine and focus light at very small lengthscales [1]. Surface plasmon polaritons (SPPs) are electromagnetic (EM) waves which are confined at a metal surface while interacting with the free electrons of the metal [2, 3]. Since the wavenumber of the light in a dielectric is larger than that of the surface plasmons at a metal-dielectric interface, it is not possible to excite SPP modes directly by illuminating the interface. However, profiling of the metal surface with corrugations allows light to couple through the patterned surface which provides the missing momentum [4–6]. Enhanced optical transmission (EOT) was achieved in a bull's eye (BE) structure comprising a single circular aperture surrounded by a periodically corrugated metal surface with concentric circular grooves [2, 7, 8]. The structure comprised of air above and below the corrugated metal surface, and transmission enhancement of up to a factor of three was obtained through the central aperture. Since the discovery of EOT phenomena in the BE structure, several structures have been investigated to achieve EOT for applications in sensing, imaging, high resolution near-field microscopy, and high density optical storage [5, 9–14]. A

#170627 - $15.00 USD Received 18 Jun 2012; revised 17 Aug 2012; accepted 26 Aug 2012; published 5 Sep 2012

two dimensional (2D) analogue of the BE structure comprising a single slit on a metal film with air above and below, symmetrically surrounded by periodic rectangular grooves, was proposed by Lezec et al [15]. Very large energy transmission enhancement was achieved by optimising the slit-to-groove distance [15] when the structure was illuminated from a normalised incident light. Recently, a metal antenna horn structure comprising periodically corrugated rectangular grooves surrounding the central slit was proposed by Guang-Yuan et al [16, 17]. In this case, oblique incident light was used to illuminate the structure and constructive interference between the SPPs excited from adjacent grooves resulted in EOT at the central slit. Corrugated surfaces have been used for many years in microwave horns to engineer their radiation patterns [18].

However, in order to integrate nano-plasmonics with silicon microelectronics, silicon based complementary-metal-oxide-semiconductor (CMOS) compatible structures are required for the plasmonic devices, including plasmon excitation and coupling structures [19]. In this paper we studied the efficiencies of a silicon-on-insulator (SOI) plasmonic coupler with grooved metallised sidewalls, in which plasmon modes are excited and focused into a narrow silicon slit. A theoretical investigation for the proposed plasmonic coupler was carried out using a 2D finite element electromagnetic model (FEEM) [20]. The physical parameters affecting the coupling efficiency into the slit were investigated and a transfer matrix model (TMM) was developed to analyse and compare the results with those obtained from the FEEM. Furthermore, the application of the optimised plasmonic coupler to achieve maximum coupling efficiency of light into a single mode dielectric waveguide was investigated. The efficiency with which light couples into two nano-slot plasmonic waveguides was also investigated, in which case the light equally splits into each of the two plasmonic slits at the apex of the structure.

2. Device geometry

A schematic view of the SOI compatible plasmonic coupler, which converges into a 30nm silicon slit, is shown in Figure 1. Transverse magnetic (TM) polarised light from a broad input opening was assumed to illuminate the structure. The incident light is projected from the same plane as that of the plasmonic coupler. The structure was symmetrically corrugated with rectangular grooves whose angle (ϕ) and period (L) were chosen to achieve maximum coupling efficiency into the slit. ϕ and L were determined by the requirements: (i) that SPPs generated by adjacent grooves are in phase and (ii) that the incident light falling on each groove is in phase [4]. The calculated values of ϕ and L that satisfied this condition were $\approx 32^{\circ}$ and $2\lambda_{spp}$ (where λ_{spp} is the SPP wavelength). ϕ remained independent of the dielectric material used in the structure and of the incident wavelength, provided the metal has a dielectric constant with a large negative real part. Optimisation of the plasmonic coupler with respect to the groove depth (D_{gr}), width (W_{gr}), number of grooves (N_{gr}), and the slit-to-nearest-groove distance (d_{sg}) was then carried out to achieve maximum coupling efficiency into the slit. In all the following simulations, silver was used as the metal with a refractive index of 0.144+11.366i [21] at 1.55 μm wavelength.

3. Finite element and transfer matrix simulation models

The power coupling efficiency into the slit was investigated for varying N_{gr} using the FEEM as shown in Figure 2. In each case, the figure shows the maximum simulated efficiency for incident wavelengths within the range 1.538-1.562 μm. All other parameters were kept fixed. For $N_{gr} > 4$, the SPPs excited from the outermost grooves and which propagate towards the slit are largely absorbed due to the increased amount of metal present, which adds to the total loss in the plasmonic coupler, hence leading to a decreasing coupling efficiency into the slit. For $N_{gr} < 3$, the size of the structure is limited, resulting in a reduced amount of metal used in the structure: therefore most of the light from the input is transmitted into the slit, resulting

#170627 - $15.00 USD Received 18 Jun 2012; revised 17 Aug 2012; accepted 26 Aug 2012; published 5 Sep 2012

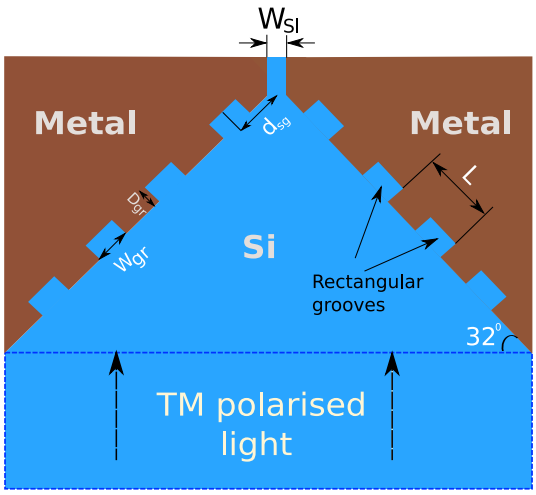

Fig. 1: Plan view of the symmetrically corrugated silicon based plasmonic coupler.

in a large coupling efficiency. However, in this case the input aperture is small, which is a disadvantage for coupling light from a broad input fibre opening. A maximum power coupling efficiency of ≥ 40 % was attained when $N_{gr} = 4$ for which the input aperture was 6.0μm. Hence, this value was used to further investigate the coupling efficiency dependence on other physical parameters.

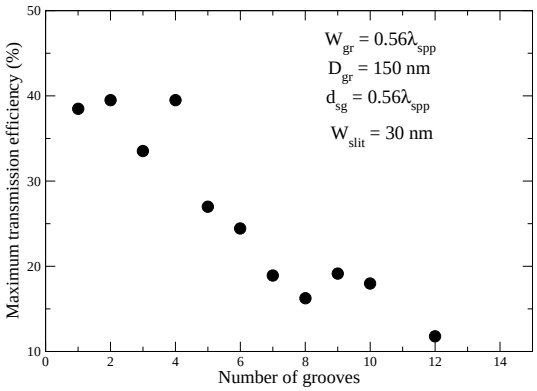

Fig. 2: Maximum power coupling efficiency to the narrow silicon slit as a function of N_{gr}.

Figure 3(a) shows maximum power coupling efficiencies as a function of D_{gr} while keeping other parameters fixed. A maximum coupling efficiency at $D_{gr} \approx 50$ nm was obtained, followed by decreasing efficiencies with a minimum at $D_{gr} \approx 70$ nm. For $D_{gr} > 70$ nm, the coupling efficiency increases again, leading to a maximum of $\approx 40\%$ for a broad range of D_{gr} varying from 120-190 nm. In addition, a second transmission minimum at $D_{gr} \approx 220$ nm was obtained. To explain this unusual transmission dependence for different D_{gr}, a transfer matrix model (TMM) was developed using parameters extracted from the FEEM. Consider an array of n identical grooves, spaced by a length L, labelled as $1, \ldots, n$, where groove 1 is nearest to the slit. The array is tilted in respect to the wavefront of the incoming free-propagating light, and the vertical spacing (along the propagation direction) between adjacent grooves is H. The wave

#170627 - $15.00 USD Received 18 Jun 2012; revised 17 Aug 2012; accepted 26 Aug 2012; published 5 Sep 2012

amplitudes on the two sides of the array can be related by a transfer matrix equation with source terms. In particular, for the right-hand side of the plasmonic coupler in Figure 1 this reads:

$$\mathbf{B}_n = (\mathbf{T}_G\mathbf{T}_L)^{n-1}\mathbf{T}_G\mathbf{A}_1 + \sum_{i=1}^{n}(\mathbf{T}_G\mathbf{T}_L)^{n-i}\exp(j(n-i)\phi)\mathbf{C_i} \tag{1}$$

where

$$\mathbf{A}_1 = \begin{bmatrix} A_1^+ \\ A_1^- \end{bmatrix}, \quad \mathbf{B}_n = \begin{bmatrix} B_n^+ \\ B_n^- \end{bmatrix}, \quad \mathbf{C_i} = \begin{bmatrix} C_i^B - rC_i^F/t \\ -C_i^F/t \end{bmatrix} \tag{2}$$

$\mathbf{A}_1$ and $\mathbf{B}_n$ are wave amplitudes on the left and right of the array, respectively, with "+"and "−"denoting waves travelling to the right or to the left; C_i^F and C_i^B are the amplitudes of plasmons travelling in the *forward* and *backward* direction (see the inset of Figure 3(d) for the convention), excited in a groove by the oblique-incidence free-propagating light. The subscript i allows different grooves to generate different amplitudes of plasmon waves because the incident light intensity may vary across the array according to the form of the TM mode assumed at the input. Furthermore,

$$\mathbf{T}_G = \begin{bmatrix} t - r^2/t & r/t \\ -r/t & 1/t \end{bmatrix} \mathbf{T}_L = \begin{bmatrix} \exp(j\beta_{SPP}L) & 0 \\ 0 & \exp(-j\beta_{SPP}L) \end{bmatrix} \tag{3}$$

are the transfer matrices for plasmon waves of the groove and flat-metal path of length L. The complex coefficients r and t in $\mathbf{T}_G$ denote the amplitude reflection and transmission coefficients of a groove (including the phase shift), while β and β_{SPP} are the propagation constants of light and plasmon waves (which are also generally complex, to allow for losses), and $\phi = \beta H$ is the phase lag of plasmons excited in adjacent grooves. In these equations, a groove is considered as a point-like (i.e. line-like, in this 2D system) scatterer, and is generally lossy; i.e, an incident plasmon can also be scattered into free light or partially absorbed, rather than being only transmitted or reflected, which implies that $|t|^2 + |r|^2 < 1$. In this formulation, the scattered radiation is effectively counted as lost and not allowed to return into the system (a more involved approach, which includes the scattered "cylindrical waves"in the transfer matrix formulation, was described recently in [22]). Eq. (1) can be written as

$$\begin{bmatrix} B_n^+ \\ B_n^- \end{bmatrix} = \begin{bmatrix} T_{11} & T_{12} \\ T_{21} & T_{22} \end{bmatrix} \begin{bmatrix} A_1^+ \\ A_1^- \end{bmatrix} + \begin{bmatrix} S^+ \\ S^- \end{bmatrix} \tag{4}$$

where $S^{+,-}$ is the collection of source terms (the sum in Eq.(1)). In the layout considered here there are no incoming plasmons to the array, i.e. $A_1^+ = 0$ and $B_n^- = 0$, and solving Eq.(4) gives the amplitudes of the outgoing plasmons travelling towards the slit (A_1^-) and away from it (B_n^+):

$$A_1^- = -\frac{S^-}{T_{22}}, \qquad B_n^+ = S^+ - \frac{T_{12}S^-}{T_{22}} \tag{5}$$

where the A_1^- component is the useful part, which carries energy towards the slit. The magnitudes of the transmission and reflection coefficients ($|t|$ and $|r|$) used in the TMM for different D_{gr} were determined by using the FEEM to study a single groove as shown in Figure 4. An in-plane SPP field was launched towards the groove and the transmitted and reflected field amplitudes were extracted at a distance of ≈ 2 μm from either side of the groove where the scattered field can be assumed to be negligible. The resulting transmission and reflection coefficients are shown in Figure 3(b). These simulations were also used to determine the phase change experienced by an SPP due to transmission or reflection by a single groove, as shown in Figure 3(c). The phase shift induced by transmission across a groove remains approximately constant for $D_{gr} > 70$nm.

#170627 - $15.00 USD Received 18 Jun 2012; revised 17 Aug 2012; accepted 26 Aug 2012; published 5 Sep 2012

The efficiency with which a single metal groove excites SPPs was obtained by simulating the illumination of a groove with TM polarised light incident at an angle of 32° (see the inset of Figure 3(d)). The excitation efficiencies of the SPPs propagating forwards and backwards (C^F and C^B respectively), relative to the direction of the incident light, were obtained by sampling the field amplitude at a large distance from the groove where the field is mostly dominated by the SPPs. Figure 3(d) shows C^F and C^B for varying D_{gr}. Figure 3(a) shows the overall power transmission efficiency obtained from the TMM for different D_{gr}. The agreement between the TMM and FEEM results is qualitative, rather than quantitative, since the approximate TMM description does not include effects such as the efficiency with which surface plasmons are coupled from the apex of the coupler into the slit itself, the scattering of light from the grooves on one side of the structure across to grooves on the opposite side, or coupling of the scattered light back into SPPs. The main purpose of the TMM is to aid understanding of the origin of the maxima and minima in the simulated coupling efficiency with respect to D_{gr}. The maximum in the coupling efficiency obtained at D_{gr}= 50 nm agrees well with that predicted by the TMM and arises from a maximum in the forward plasmon excitation efficiency by each groove and a minimum in the backward excitation efficiency (Figure 3(d)). For $D_{gr}\approx$ 70 nm, the FEEM results exhibit a minimum transmission coupling efficiency, and the TMM indicates that this is due to a minimum in the transmission coefficient (Figure 3(b)), (and a maximum in the reflection coefficient) for SPPs arriving at each groove, combined with a maximum in the backward SPP excitation efficiency (Figure 3(d)).

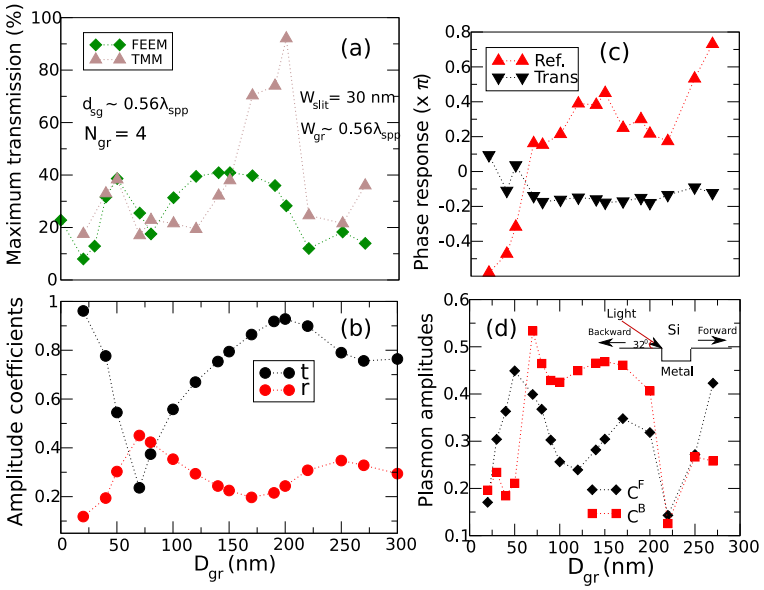

Fig. 3: (a) Maximum transmission coupling efficiency obtained in the narrow silicon slit for different D_{gr} using the FEEM (green diamonds) and TMM (brown triangles). (b) The SPP transmission and reflection coefficients obtained from a planar Si-metal structure comprising a single groove for different D_{gr}. (c) SPP transmission and reflection phase shifts for different D_{gr}. (d) Excitation efficiencies of SPPs at a single Si-metal groove, propagating forwards (C^F) and backwards (C^B) relative to the incident light direction. The inset at the top right shows a cross section of the structure used for these simulations: a planar Si-metal bilayer containing a single groove illuminated by an obliquely incident light beam.

To investigate the transmission response of a single groove, we simulated the electric field

#170627 - $15.00 USD Received 18 Jun 2012; revised 17 Aug 2012; accepted 26 Aug 2012; published 5 Sep 2012

profiles (E_y) which occur when an SPP mode passes across a metal/silicon groove, for a range of groove depths. As the groove becomes deeper, interaction of the field with the leading edge of the groove increases, causing both strong scattering and reflection (as shown in Figure 4(a)), which result in a transmission minimum for D_{gr} = 70nm. As the groove depth is further increased, the scattering effect diminishes and the mode is progressively less perturbed by the groove, with a transmission maximum observed for D_{gr} = 200nm (Figure 4(b)). For groove depths in this range, the groove appears to support a first-order vertical resonant mode, for which condition the mouth of the groove is best matched to the adjacent metal plane. However, this resonance has very low selectivity, due to the relatively large width of the groove. It should be noted that the nature of groove modes is strongly dependent on the overall groove profile (c.f. Ref. [23]).

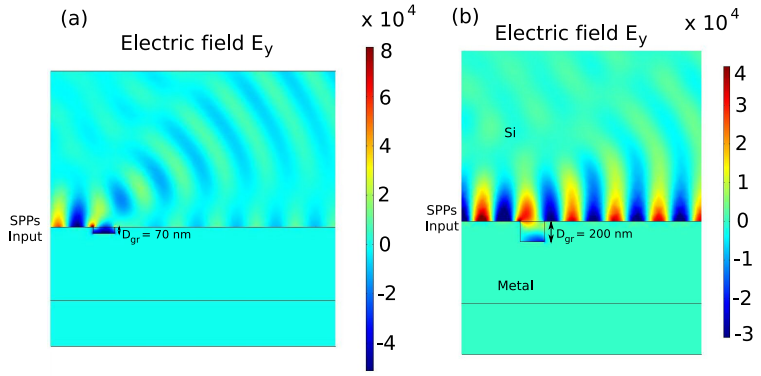

Fig. 4: Surface plasmon electric field profile (E_y) in a planar Si-metal structure comprising a single groove for (a) D_{gr} = 70nm and (b) D_{gr} = 200nm.

For D_{gr}= 220nm, a second minima in the overall power transmission coupling efficiency was obtained in the FEEM result, which agrees well with that from the TMM result (Figure 3(a)). The TMM study indicates that this behaviour is due to a minimum in the excitation efficiency of forward propagating plasmons by each groove (Figure 3(d)). A very weak lateral resonance at D_{gr}=220nm was obtained compared to the strong lateral SPP resonances within the groove at D_{gr}= 200 and 250nm, which resulted in a minimum excitation efficiency in both the forward and backward propagating SPP waves. In contrast, the transmission and reflection are far less sensitive to the precise value of D_{gr}.

4. Optimisation

Figure 5(a) shows the maximum power coupling efficiencies obtained for varying W_{gr} while keeping other physical parameters fixed. The figure predicts a broad range of groove widths (0.5-0.6λ_{spp}) for which maximum coupling efficiency occurs. Figure 5(b) shows the electric field profile (E_x) for W_{gr} = 0.56λ_{spp} where strong lateral resonance SPP modes are formed within the first and third grooves (from the slit) and weaker lateral resonances occur within the second and fourth grooves. The simulation results predicted a maximum power coupling efficiency of $\approx$ 62% for W_{gr} = 0.56λ_{spp}. This value agrees well with the range of W_{gr} (0.5-0.6 λ_{spp}) required to achieve EOT in a 2D BE structure [13].

However, the other maxima at $W_{gr} \approx 0.35\lambda_{spp}$ and $0.8\lambda_{spp}$ shown in Figure 5(a) are not the result of individual groove resonances but arises from the optimum collective behaviour of the 2x4 rectangular groove array. Figures 6(a) and (b) show magnified views of the electric field

#170627 - $15.00 USD Received 18 Jun 2012; revised 17 Aug 2012; accepted 26 Aug 2012; published 5 Sep 2012

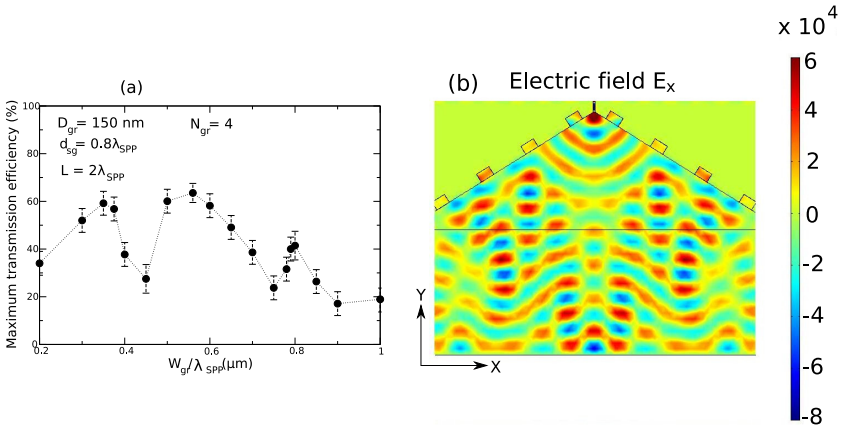

Fig. 5: (a) Power coupling efficiency into the silicon slit as a function of W_{gr}. The error bars signify the variation in FEEM results with respect to the mesh definition in the simulation domain (this convention is also used in other figures). (b) Magnified view of the SPP electric field profile at W_{gr}= 0.56λ_{spp}.

profile (E_y) for $W_{gr} \approx 0.35$ and $0.45\lambda_{spp}$, which correspond to the first maxima and minima in the coupling efficiency in Figure 5(a). It can be seen from the figures that the SPP field intensity within the groove nearest to the slit can influence the power coupling efficiency into the slit. At $W_{gr} \approx 0.35\lambda_{spp}$, the SPP propagation is least influenced by the presence of the groove resulting in an enhanced coupling efficiency (Figure 6(a)) into the slit. In contrast, for $W_{gr} \approx 0.45\lambda_{spp}$, strong absorption of the pinned SPP mode occurs within the groove resulting in a reduced coupling efficiency. A similar behaviour of the electric field intensity within the groove was found for W_{gr} = $0.75\lambda_{spp}$ and $0.8\lambda_{spp}$ where a stronger field intensity was obtained in the former than the latter case, resulting in a larger coupling efficiency for W_{gr} = $0.8\lambda_{spp}$.

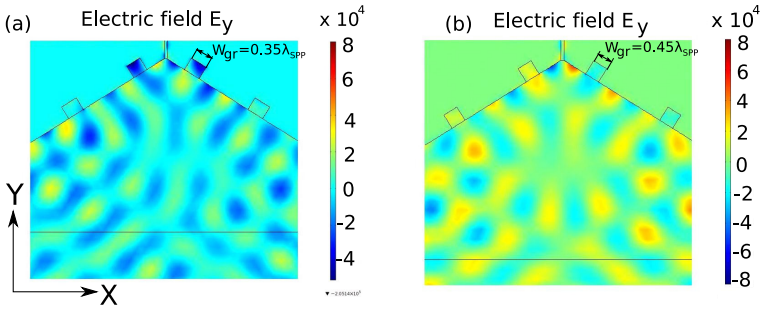

Fig. 6: Magnified views of the electric field (E_y) profile for (a) $W_{gr} \approx 0.35\lambda_{spp}$ and (b) $W_{gr} \approx 0.45\lambda_{spp}$

Next, the distance between the centres of the slit and the nearest groove (d_{sg}) was optimised such that the SPPs arriving at the entrance of the slit from the two sides of the coupler interfere constructively with the plasmon mode excited directly by light incident on the slit (the effective aperture of which encompasses part of the angled metal sidewalls at the apex of the coupler). Figure 7(a) shows the power coupling efficiencies for different d_{sg} obtained using the FEEM, with all other parameters kept constant. Previously, a 2D BE structure illuminated with nor-

#170627 - $15.00 USD Received 18 Jun 2012; revised 17 Aug 2012; accepted 26 Aug 2012; published 5 Sep 2012

mally incident light was predicted to have an optimum d_{sg} of $0.54\lambda_{spp}$ [13]. This path length compensates for the difference in the phase shifts introduced when the incident light generates plasmons (i) at a groove and (ii) at the slit, and also the phase shift introduced when the plasmons arriving from the groove array are coupled into the perpendicular slit (see Figure 7(b)). However, in our structure, the central slit is tilted at 32° to the normal as shown in Figure 7(c). We therefore carried out EM simulations of both cases, in which SPPs were launched along a planar metal surface towards a single slit, in order to determine the difference in phase shifts for coupling into a perpendicular, relative to a 32° tilted slit. The simulated difference in the phase shifts was $\approx 0.7\pi$, and we therefore expected optimum coupling efficiency to occur when d_{sg} was increased by $(0.7/2)\lambda_{spp}$ relative to the 2D BE case (i.e. at $d_{sg} = 0.858\lambda_{spp}$). This agrees well with the FEEM results shown in Figure 7, in which a maximum power coupling efficiency of ≈63% was attained for $d_{sg} = 0.85\lambda_{spp}$.

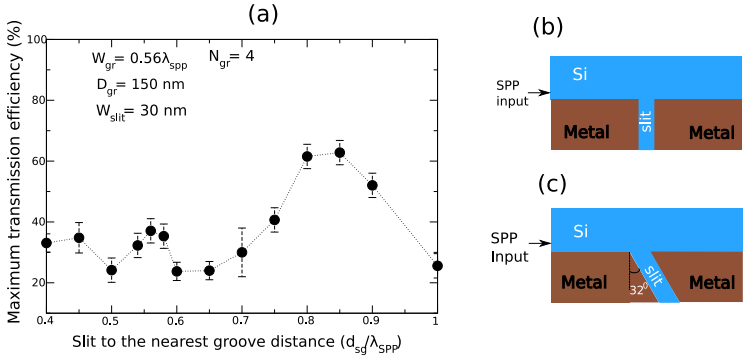

Fig. 7: (a)Effect of the slit to nearest groove distance (d_{sg}) on the maximum power coupling efficiency. (b) Schematic diagram of a right angled slit in the case of a 2D BE structure and (c) a tilted slit in the proposed silicon-based plasmonic coupler.

Figure 8(a) shows the dependence of the coupling efficiency on the width of the slit (W_{Sl}) at the apex of the optimised plasmonic coupler as predicted by the FEEM. All the other physical parameters were kept fixed. For a deep subwavelength slit ($W_{Sl} < 30$nm), the pinned SPP mode at the metal-dielectric interface superposes with the incident dielectric mode at the vicinity of the slit entrance, which is efficiently converted into the SPP mode supported by the narrow slit (Figure 8(b)), resulting in a maximum coupling efficiency of 72% for W_{Sl}= 20nm. In addition, the SPP propagation appeared to be least affected by the presence of the grooves, which in turn aids in an enhanced coupling into the slit. However, the above phenomena decrease with increasing W_{Sl} up to 60nm, beyond which the coupling efficiency again increases (Figure 8(a)). For $W_{Sl} > 150$nm, strong lateral SPP resonant modes are pinned at the sidewalls within the groove nearest to the slit (Figure 8(c)), which results in large coupling efficiencies in the range of ≈66-75% (Figure 8(a)). Whilst the results were obtained using 2D simulations, which neglect any leakage of the EM mode above and below the metallised sidewalls of the structure, previous simulation work on plasmonic modulators [28] implies that this leakage is likely to be small for device heights $>$ 150nm.

5. Applications to SOI waveguide coupling and plasmon-mode splitting

The efficiency with which the silicon-based plasmonic coupler couples light from a broad input opening into a single mode SOI waveguide was investigated using the FEEM. Previous studies

#170627 - $15.00 USD Received 18 Jun 2012; revised 17 Aug 2012; accepted 26 Aug 2012; published 5 Sep 2012

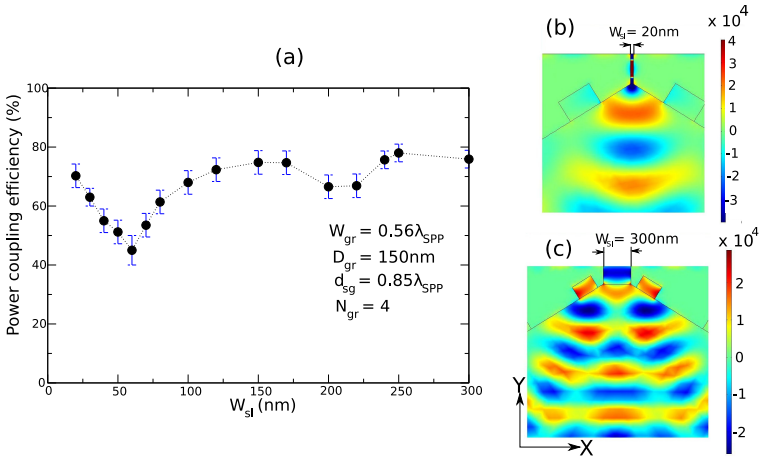

Fig. 8: (a) Simulated power coupling efficiency of the optimised plasmonic coupler as a function of W_{Sl}. Simulated electric field (E_x) profile of the plasmonic structure coupling into (b) a 20nm slit and (c) a 300nm wide slit.

on coupling a fibre to an SOI waveguide have considered an end-fire inverted taper with a coupling loss of $\approx$ 4.5dB using an 8μm wide and 400μm long tapered waveguide [24]. For an out of plane fibre grating coupler, the measured coupling loss from a standard fibre to a single mode SOI waveguide was 5.2dB, using a 50μm taper length [25]. Here, we investigate the prospect of using the optimised plasmonic coupler to couple light from wide input optical fibre grating into an SOI waveguide with low loss over micron-scale taper lengths.

Based on the simulated results obtained above, an optimised structure was employed to achieve maximum power coupling efficiency into a 300nm SOI waveguide. Figure 9 shows the electric field profile (E_x) of the simulated structure. SPP modes are pinned on each wall of the 300nm metal-Si-metal slit at the apex of the coupler. These modes are efficiently coupled into a dielectric mode of the SOI waveguide. The FEEM predicted maximum coupling efficiencies of $\approx$63% and 61.5 % in plasmonic couplers comprising 4 and 7 grooves respectively, which correspond to input opening widths of 6.4 and a 10.4 μm. The taper lengths of these structures are only 1.85 and 3.15μm. A standard single mode optical fibre has a typical core diameter of $\approx$10 μm at a 1.55 μm wavelength [26]. This means that the proposed plasmonic coupler can be employed for coupling light from a fibre grating into either a nano-plasmonic waveguide or a single mode SOI waveguide with $\approx$ 2.1 dB insertion loss.

Finally, we investigated the performance of the plasmonic coupler as an optical splitter in which the incoming light from a broad input opening is coupled equally into two nano-slit plasmonic waveguides. The two nano-slits are separated by a metal gap region as shown in the inset of Figure 10. The width of the gap (W_{gap}) was varied while keeping the rest of the parameters fixed and the splitting efficiency of the coupled power into each slit was determined using the FEEM. Figure 10 shows the dependence of the power splitting efficiency into each 50nm nano-slit as a function of W_{gap}. The splitting efficiency into each slit is not very sensitive to the variation of W_{gap} for widths up to 50nm, beyond which the sensitivity increases. Since the optical path length of the SPPs propagating along one side of the coupler is different upon arrival at the entrance of the two slits, the condition for achieving maximum constructive interference between SPPs at the slit entrance degrades with increasing W_{gap}. The total SPP intensity is proportional to the cosine squared of the phase difference, which is why it is not very sensitive to

#170627 - $15.00 USD Received 18 Jun 2012; revised 17 Aug 2012; accepted 26 Aug 2012; published 5 Sep 2012

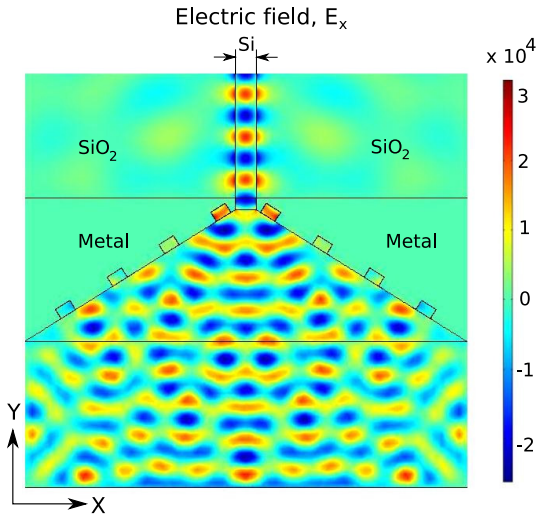

Fig. 9: Electric field profile (E_x) of the silicon based plasmonic structure coupling into a 300nm wide single mode dielectric waveguide.

W_{gap} for smaller values, up to 50nm, but degrades for $W_{gap} >$ 50nm. Additionally, absorption of the pinned SPPs modes by the metal increases with increasing W_{gap}: however, this has a far smaller effect on the overall system performance. Simulation results predicted a maximum power coupling efficiency of 36.5% (or a total coupling efficiency of ≈73%) into each 50nm SOI nano slit.

The proposed silicon based plasmonic coupler can be realised on an SOI substrate using e-beam lithography to define the coupler geometry, followed by Si etching and self aligned metal sidewall deposition. Finally, a covering oxide layer should be deposited. Since the thickness of the metal does not affect the system performance, the metal surrounding the grooves and the slit need not to be of uniform thickness.

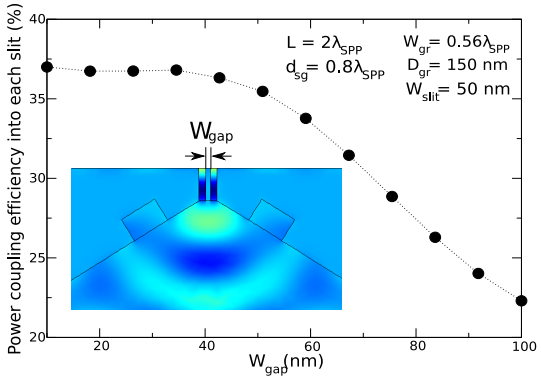

Fig. 10: Simulated power coupling efficiency into each slit as a function of varying W_{gap}. The inset shows the magnified view of the electric field profile (E_x) of the silicon-based plasmonic splitter coupling into two 50nm wide nano-slit waveguides.

#170627 - $15.00 USD Received 18 Jun 2012; revised 17 Aug 2012; accepted 26 Aug 2012; published 5 Sep 2012

6. Conclusion

In summary, we have investigated the performance of a silicon based plasmonic coupler which comprises grooved metal side walls tapering into a nanoscale metal-silicon-metal plasmon waveguide at the apex of the structure. Various geometric features including the taper angle and period of the grooves were investigated and a transfer matrix model was developed to identify the principal electromagnetic phenomena which determined the coupler performance. The structure can be applied not only to couple light into a single nano-scale plasmonic waveguide with $\approx$ 72% coupling efficiency, but also to achieve efficient coupling into a single mode dielectric strip waveguide, and to achieve simultaneous coupling and splitting of an input signal into two equivalent plasmon waveguides with an insertion loss of 1.31 dB. A significant advantage of the structure is that its total length is very short– less than a third of the input aperture width. The proposed plasmonic coupler therefore promises to be a key component in future on-chip plasmonic optical circuits for coupling light directly from a large area fibre grating into a nanoscale plasmonic waveguide. Furthermore, the capability of the structure to provide simultaneous coupling and splitting into two equivalent plasmonic waveguide means that it could be used to couple an optical carrier directly into an Mach-Zehnder plasmonic modulator [27, 28], hence providing a high efficiency passive front end for an on-chip plasmonic transceiver.

Acknowledgments

The work has been funded by the Engineering and Physical Sciences Research Council (EPSRC) program, UK Silicon Photonics. The authors would like to thank Dr. N.J. Pilgrim for useful discussion.

#170627 - $15.00 USD Received 18 Jun 2012; revised 17 Aug 2012; accepted 26 Aug 2012; published 5 Sep 2012